Pergamon

0956-7151(94)E0004-Z

Acta metall. mater. Vol. 42, No. 6, pp. 1933–1945, 1994

0956-7151/94 $7.00 + 0.00

MATRIX CRACKING OF CROSS-PLY CERAMIC COMPOSITES

Z. C. XIA and J. W. HUTCHINSON

Division of Applied Sciences, Harvard University, Cambridge, MA 02138, U.S.A.

(Received 22 October 1993)

Abstract—A micromechanics study is presented of the matrix cracking behavior of laminated, fiber-reinforced ceramic cross-ply composites when subject to tensile stressing parallel to fibers in the 0° plies. Cracks extending across the 90° plies are assumed to exist, having developed at relatively low tensile stresses by the tunnel cracking mechanism. The problem addressed in this study is the subsequent extension of these intital cracks into and across the 0° plies. Of special interest is the relation between the stress level at which the matirx cracks are able to extend all the way through the 0° plies and the well known matrix cracking stress for steady-state crack extension through a uni-directional fiber-reinforced composite. Depending on the initial crack distribution in the 90° plies, this stress level can be as large as the uni-directional matrix cracking stress or it can be as low as about one half that value. The cracking process involves a competition between crack bridging by the fibers in the 0° plies and interaction among multiple cracks. Crack bridging is modeled by a line-spring formulation where the nonlinear springs characterize the sliding resistance between fibers and matrix. Crack interaction is modeled by two representative doubly periodic crack patterns, one with collinear arrays and the other with staggered arrays. Material heterogeneity and anisotropy are addressed, and it is shown that a homogeneous, isotropic average approximation can be employed. In addition to conditions for matrix cracking, the study provides results which enable the tensile stress–strain behavior of the cross-ply to be predicted, and it provides estimates of the maximum stress concentration in the bridging fibers. Residual stress effects are included.

1. INTRODUCTION

The process by which a fiber-reinforced cross-ply ceramic composite is damaged and eventually fails under tension is very complex. When the tensile stress is applied along one of the fiber directions, one often observes an overall stress–strain response as schematically illustrated in Fig. 1. After an initial elastic response, the damage starts with matrix cracking in the 90° plies. These cracks spread as 3D tunneling cracks from small flaws located in the matrix of the 90° plies, and generally arrest at the interfaces between 0°/90° plies before spreading into the adjacent 0° plies [1]. With further increase of the applied stress, more tunneling cracks develop in the 90° plies until they saturate. At about this stage, the fully tunneled cracks begin to extend into the adjacent 0° plies without fiber failure and extend until they overlap. The matrix cracks eventually coalesece at even higher stress with the matrix of the laminate being fully cracked. The intact fibers in the 0° plies, which are now carrying all the load, fail at the fiber bundle fracture stress $c_f S/2$.

The matrix cracking in the 90° plies has been a subject of research efforts for the past two decades. While most of the work in this area deals with the effect of matrix cracking on the degradation of the stiffness of the laminate (for example, as reviewed in [2]), relatively less has been done to relate the full details of the overall stress–strain response to the constituent properties of the laminate. An attempt along this direction was recently made in [3] where the concept of steady-state tunneling cracks was employed to model matrix cracking as a three-dimensional process. The minimum tensile stress required for the onset of tunneling cracks (the start of nonlinearity in Fig. 1) was predicted. The evolution of the crack density in the 90° plies was related to the applied stress, and the overall stress–strain behavior (from onset to saturation of the tunneling cracks in the 90° plies) was obtained as a function of the basic geometry of the composite, the toughness of the matrix, and the residual stress between plies.

The next logical step is to investigate subsequent damage where matrix cracks spread into the neighboring 0° plies. This is an unavoidable step if progress is to be made in the effort to understand the complete tensile behavior of a laminated cross-ply composite. Several new considerations come into play. Firstly, the matrix cracks are partially bridged by intact fibers in the 0° plies. The fiber-bridged length of the crack is comparable to the unbridged length (the 90° ply thickness), and small scale bridging (SSB) does not apply. To fully solve this problem, a rigorous large scale bridging (LSB) analysis is required. Recent research efforts on this general topic can be found in

[4, 5], where the main concern centered on the tensile strength of unidirectional fiber-reinforced ceramic composites containing a single crack-like flaw. Secondly, interaction among multiple cracks plays an important, and, sometimes even critical, role in the crack growth process. The modeling of the process under large scale bridging conditions has not been addressed. Lastly, the laminated composites are anisotropic and heterogeneous in nature. The importance of material anisotropy and heterogeneity on the fracture performance of such laminates must also be addressed.

To provide some quantitative feel for the damage sequence of a cross-ply laminate under tensile loading, we take as an example the CAS/SiC laminate system used in the experiments in [1]. It consists of Nicalon fibers in a calcium–alumino–silicate matrix in a cross-ply configuration. The constituent properties are

$$E_m = 97\ \text{GPa}, \quad E_f = 200\ \text{GPa}, \quad c_f = 0.37,$$

$$R = 7.5\ \mu\text{m}, \quad \Gamma_m = 25\ \text{J/m}^2, \quad \tau = 20\ \text{MPa}$$

and the half ply thickness t is 90 μm. Two types of residual stresses exist in the laminate, introduced during manufacturing process because of mismatch of the thermal properties of fibers and matrix. One is the overall residual stress between different plies which was measured to be approximately 30 MPa in tension perpendicular to the fibers in the 90° plies, and about same amount of compression in the 0° plies acting parallel to the fibers. At a smaller scale within each layer is the residual stress between fibers and matrix which has both an axial and radial component. The measured residual stress in matrix in the axial direction is $\sigma_R^m = 100 \sim 120$ MPa. Based on the above information, we can evaluate several important stress quantities, which are also indicated on the ordinate of Fig. 1:

1. σ_{onset}, the stress for onset of tunneling cracking (the formula is given in [3]). This stress sets the condition under which matrix cracking first can occur in the 90° plies. Accurate prediction of σ_{onset} requires knowledge of the toughness of the 90° plies in the tunneling mode. An estimated value of σ_{onset} for the above CAS/SiC system is around 80 MPa. Since there exists a residual tension of 30 MPa in the 90° plies, the net applied stress σ needed for the onset of tunneling cracking will be around 50 MPa [3].

2. σ_0, a stress quantity measuring the condition at which plane strain cracks in the 90° plies begin to spread into the neighboring 0° plies. It is one of the basic parameters in this study, and it will be introduced in more detail later in the development. The calculated σ_0 from equation (6) (see below) is 88 MPa. The residual tension in the 90° plies will lower the net applied stress to about 58 MPa.

3. σ_{mc}, the steady-state matrix cracking stress for a *uni-directional composite* [6, 7]. It is the other basic stress parameter used in this study. It depends on the matrix toughness and the bridging capabilities of the fibers. It is given by equation (5) in next section and is calculated to be 323 MPa. Since there exists a residual tension in matrix in the amount of $\sigma_R^m = 100 \sim 120$ MPa, the critical applied stress needed to advance the steady-state matrix crack will be in the range 156–184 MPa. This range of the value is consistent with the experimentally measured range of 140–160 MPa in [1]. One of the main objectives of this paper is to determine the relation between σ_{mc} for the uni-directional composite and the stress at which matrix cracks first cross the 0° plies in the cross-ply composite.

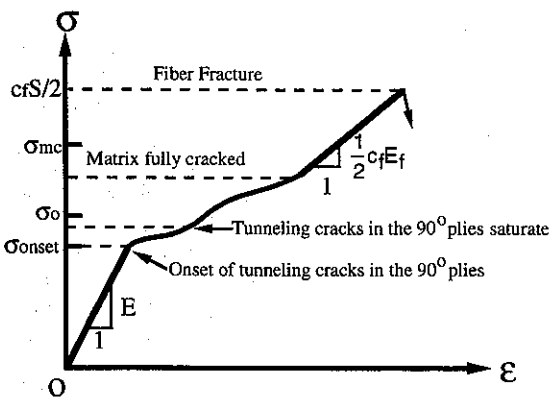

Fig. 1. A schematic illustration of stress–strain curve for a cross-ply laminate under tensile loading.

The above three stress values support the illustration in Fig. 1 of the damage process in a cross-ply laminate. Similar behavior was reported in [1] based on their experimental observations.

Thus, the aim of the present work is a micromechanics investigation of the tensile behavior of a laminated fiber-reinforced cross-ply ceramic composite with matrix cracks in the 90° plies penetrating into the adjacent 0° plies. As emphasized, it should be regarded as a continuation of the work of [3] on tunnel cracking in the 90° plies. Here, the main focus will be on the constraining effect of bridging fibers and the interaction among multiple cracks during the crack growth process. The overall tensile behavior of such laminates will be determined. We first examine the problem of material anisotropy and heterogeneity, and demonstrate that anisotropy can be accounted for in a simple manner such that accurate approximate solutions can then be generated from results for a homogeneous, isotropic material. The effect of bridging fibers is modeled as distribution of nonlinear springs obeying a traction-separation law characterizing fibers slipping relative to the matrix under a constant friction stress τ. Two doubly periodic crack patterns are analyzed in order to

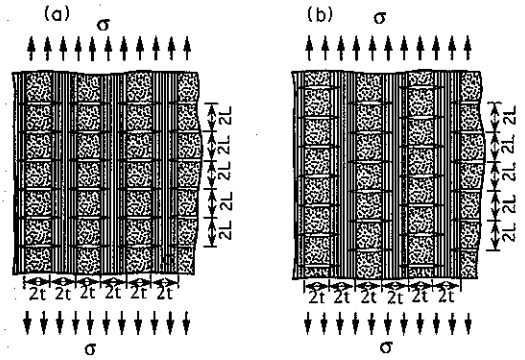

Fig. 2. Two representative doubly periodic crack patterns. (a) Collinear arrays. (b) Staggered arrays.

understand interactions among cracks, one, a collinear pattern [Fig. 2(a)] and the other, a staggered pattern [Fig. 2(b)]. The collinear pattern models the extreme situation where stres intensity enhancement due to interactions is maximal. The staggered pattern represents perhaps a more realistic situation in which overlapping of matrix cracks in the 0° plies will occur. This type of pattern, opposed to the collinear pattern, models the more or less random development expected for the tunnel cracks in the 90° plies. Also investigated in this work is the stress concentration in the bridging fibers. This is an important issue because failure of bridging fibers constitutes the ultimate failure mechanism for these composites.

The paper is organized as follows. We begin with a general description of the problem including the fiber bridging model, and go on to demonstrate the validity of the scheme for accounting for the laminate anisotropy using results from plane strain isotropy. The body of paper is devoted to the presentation and discussion of the crack growth process and overall tensile behavior for each of the two crack patterns. The applied tensile stress and extra strain due to the crack growth process are presented for various crack densities, together with the stress concentration in bridging fibers. The role of residual stresses introduced during the manufacturing process is also illustrated and discussed. The mathematical formulation and numerical solution procedure are detailed in the Appendices. A numerical example for the above mentioned CAS/SiC laminate is given in the last section as an illustration. The predicted secant modulus as a function of the applied stress is compared with experiment data reported in [1].

2. CHARACTERIZATION OF THE PROBLEM

2.1. An approximation accounting for the anisotropy of the laminate

Previous studies usually take a uni-directional fiber-reinforced composite to be transversely isotropic about the fiber directions. With fibers aligned with the 1-axis, the constitutive relation for an undamaged ply is

$$\epsilon_{11} = \frac{1}{E_L}\sigma_{11} - \frac{\nu_L}{E_L}(\sigma_{22}+\sigma_{33})$$

$$\epsilon_{22} = -\frac{\nu_L}{E_L}\sigma_{11} + \frac{1}{E_T}\sigma_{22} - \frac{\nu_T}{E_T}\sigma_{33}$$

$$\epsilon_{33} = -\frac{\nu_L}{E_L}\sigma_{11} - \frac{\nu_T}{E_T}\sigma_{22} + \frac{1}{E_T}\sigma_{33}$$

$$\epsilon_{23} = \frac{1}{2\mu_T}\sigma_{23} \quad \sigma_{13} = \frac{1}{2\mu_L}\sigma_{13} \quad \sigma_{12} = \frac{1}{2\mu_L}\sigma_{12} \qquad (1)$$

where the subscript L stands for longitudinal properties and the subscript T stands for transverse properties. All the elastic properties can be calculated either on the basis of the Hill [6] self-consistent model or from other models.

The anisotropic effect for a unidirectional fiber-reinforced composite can be characterized by an orthotropy factor [5]. However, it is less clear how one should account for the heterogeneous nature of a cross-ply associated with the two orientations of layers. For most ceramic composites, the ratio E_f/E_m of the fiber modulus to the ceramic matrix modulus ranges generally from 1 to 5. To obtain some insight into the role of material anisotropy and heterogeneity, finite element analysis of single and multiple cracking have been performed for several typical values of E_f/E_m and fiber volume fractions c_f of a

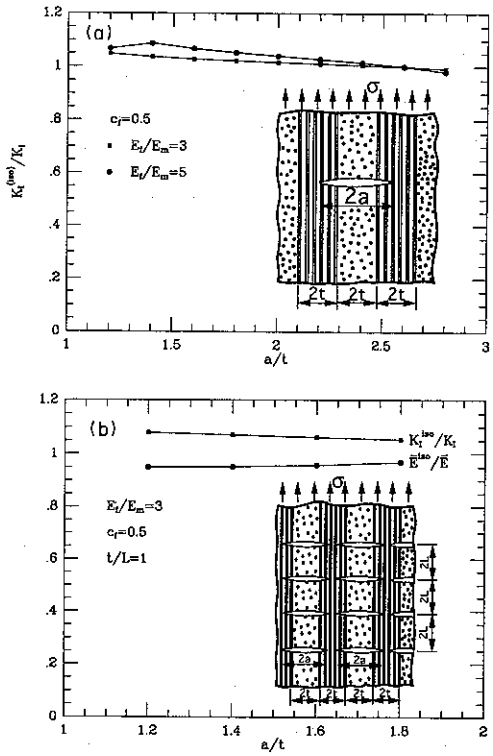

Fig. 3. Demonstrations of the validity of isotropic average approximation. (a) An isolated crack. (b) Doubly periodic cracks.

laminated composite. Two plane strain crack configurations have been analyzed as shown in the inserts of Fig. 3(a, b), with crack tips located in the 0° plies. No bridging tractions are applied. For each geometrical configuration and loading, two sets of material properties are adopted for the calculations. For the first set, the stress–strain behavior of each of the plies is taken to be elastically orthotropic obeying (1), with due regard for the two orientations. For the second set, the composite is approximated to be homogeneous and isotropic, with an overall Young's modulus E and Poisson's ratio ν given by

$$E=\frac{\frac{1}{4}\left(1+\frac{E_L}{E_T}\right)^2-\nu_L^2}{\frac{1}{2}\left(1+\frac{E_L}{E_T}\right)\left(\frac{1}{E_T}-\frac{\nu_L^2}{E_T}\right)}$$

$$\nu=\frac{2\nu_L}{1+\frac{E_L}{E_T}}$$

$$\bar{E}=\frac{E}{1-\nu^2}. \tag{2}$$

As introduced in [3], E is the uniaxial modulus of the composite in a direction parallel to either set of fibers, while ν is the Poisson's ratio associated with the out-of-plane strain component. Thus, $\bar{E}$ defined above, is the modulus governing plane strain tension parallel to the fibers in the 0° plies (with the out-of-plane strain imposed to be zero). Since the results of interest here are quite insensitive to the value chosen for the in-plane Poisson's ratio, we have also used the value ν given above as the in-plane ratio.

The calculated ratios of mode I stress intensity factors from the two calculations, K_I^{iso}/K_I, for the single crack problem are plotted in Fig. 3(a), where the geometrical configuration is shown. The Poisson's ratios of both fibers and matrix are taken to be 0.2 and the fiber volume concentration is 0.5. The deviation from unity reflects the error of the isotropic average approximation for K_I to that obtained from the anisotropic, heterogeneous model. Similar results for a doubly periodic crack pattern are shown in Fig. 3(b), where ratios of both stress intensity factors and compliances are shown. As indicated in Fig. 3(a,b), the errors introduced by the isotropic average approximation to the stress intensity factor and compliance for all practical ranges of E_f/E_m are within 8%. As cracks become longer in the 0° plies, it is seen that the errors are further reduced. This indicates that the isotropic average approximation with elasic properties defined in (2) involves little error for the study of fracture performance with cracks spanning both the 90° and the 0° plies. The major advantage of the isotropic average approximation is that it permits one to use analytical techniques and results to set up the computational problems. In this work we have used integral equation methods which employ kernels derived using complex variable methods of elasticity.

The generally adopted criterion for the growth of matrix cracks in the 0° plies is that the average energy release rate along the crack front remain equal to the critical value $c_m\Gamma_m$, where Γ_m is the matrix toughness (for example, [5, 7, 8]). The mode I intensity toughness, K_{Ic}, for the crack tip located in the 0° plies is [5]

$$K_{Ic}=\sqrt{\frac{AE_L}{1-\nu_L^2}c_m\Gamma_m} \tag{3}$$

where A is the orthotropy factor characterizing the effect of orthotropy of the 0° plies. This result follows from the formula given in [9] for the energy release rate of an orthotropic material in terms of stress intensity factor. The value of A for a wide range of E_f/E_m and c_f of fiber-reinforced ceramic composite has been calculated and presented in [5] based on Hill's self consistent model. For all practical ceramic composites, it falls between 0.84 and 1.0.

2.2. *Characterization of bridging fibers*

As in most previous studies, the debonding energy between the fibers and the matrix is ignored and sliding between the fibers and the matrix takes place when the interfacial shear stress exceeds the friction stress τ. When slip lengths are relatively large, as is often the case for many ceramic fibrous composites, the bridging fiber stress $p(x)$ is related to the crack opening displacement $\delta(x)$ by [10]

$$p(x)=\left\{\frac{2E_fE_L^2c_f^2\tau}{RE_m^2c_m^2}\delta(x)\right\}^{1/2}. \tag{4a}$$

If residual stresses between fibers and matrix are present, the above fiber bridging law can be easily modified by an extra term [11] such that

$$p(x)=\left\{\frac{2E_fE_L^2c_f^2\tau}{RE_m^2c_m^2}\delta(X)\right\}^{1/2}-\frac{E_L}{E_m}\sigma_R^m \tag{4b}$$

where σ_R^m is the average residual stress parallel to the fibers in the uncracked matrix.

The matrix cracking stress σ_{mc}, defined as the tensile stress required for the steady-state propagation of a single, long matrix crack in unidirectional fibrous composites is given by [7, 8]

$$\sigma_{mc}=\left\{\frac{6E_fE_L^2c_f^2\tau}{RE_m^2c_m}\Gamma_m\right\}^{1/3}. \tag{5}$$

In the presence of residual stress, the critical applied stress needed to advance the steady-state matrix crack is given by a modification similar to that in (4b) as $\sigma_{mc}-(E_L/E_m)\sigma_R^m$ [8].

The remaining important stress quantity to be introduced is

$$\sigma_0=\frac{K_{Ic}}{\sqrt{\pi t}} \tag{6}$$

where t is the half thickness of each ply. Under the isotropic average approximation for the composite,

σ_0 is the remote tensile stress required for the initiation of propagation into the adjacent 0° plies of an isolated pre-existing matrix crack in a 90° ply. For multiple cracks such as those in Fig. 2, the stress at which the cracks will begin advancing into the 0° plies will usually be lower than σ_0 due to crack interaction. It is worth noting that this initiation stress depends only on σ_0 and the crack configuration for the reason that the cracks are not yet bridged at this stage.

2.3. Description of the crack growth process

Now suppose the matrix cracks in the 90° plies are fully tunneled and saturated as has been analyzed in [3]. Under further increase of applied tensile stress σ, these cracks will spread into the neighboring 0° plies under plane strain conditions. The 0°/90° interfaces are assumed to be perfectly bonded. Neither delamination nor splitting along interfaces of the plies or the fiber/matrix occurs. The bridging fibers in the 0° plies are assumed to remain intact throughout the crack growth process.

Consider a cross-ply laminate subject to in-plane tensile loading only. We shall analyze the two representative crack patterns, where plane strain matrix cracks have already formed in the 90° plies, which are shown in Fig. 2 and which were introduced earlier. Suppose all cracks are growing quasi-statically in the same manner, with current crack length $2a$. The average tensile stress σ applied remotely is determined by imposing the condition that the mode I stress intensity factor K_I maintain the critical value K_{Ic} as defined in (3). This large scale bridging problem is intrinsically nonlinear. It has been solved rigorously by formulation of a nonlinear singular integral equation which is solved by iteration. The logarithmic singularity of the crack opening displacement gradient at the bridging/unbridging point (i.e. at the 90°/0° interface) is explicitly accounted for in the formulation. Mathematical details can be found in the Appendices.

The solution to this problem, in the absence of pre-existing residual stresses, is found to be completely determined by the crack geometry and a non-dimensional quantity $\sigma_0/(\beta\sigma_{mc})$, which encompasses information about both materials and the fiber bridging constraint. The material parameter β is given by (see Appendix A)

$$\beta = \left\{\frac{AE_L}{\bar{E}(1-\nu_L^2)}\right\}^{1/3} \tag{7}$$

which arises in the isotropic average approximation. For all practical fibrous composites, β is very close to 1, and reduces to 1 if the fibers and matrix have identical elastic properties. For the CAS/SiC system discussed before, $\beta = 0.998$. For a given laminated ceramic composite, $\sigma_0/(\beta\sigma_{mc})$ measures the relative compliance of the fiber bridging law. A larger value of $\sigma_0/(\beta\sigma_{mc})$ represents softer bridging, while smaller values give stronger bridging. The CAS/SiC system that Beyerle *et al.* [1] used in their experiments has $\sigma_0/(\beta\sigma_{mc}) = 0.27$. Results will be presented for $\sigma_0/(\beta\sigma_{mc})$ in the range from 0.1 to 1.0 to cover all practical cases.

In non-dimensional form, the average tensile stress σ applied remotely during the crack growth process can be expressed as

$$\frac{\sigma}{\beta\sigma_{mc}} = F_1\left(\frac{a}{t}, \frac{\sigma_0}{\beta\sigma_{mc}}, \frac{t}{L}\right) \tag{8}$$

where a/t is the non-dimensional current crack length, and t/L is the crack density as defined in either Fig. 2(a) or (b). The extra overall tensile strain $\Delta\epsilon$ (i.e. the inelastic strain), caused by the presence of the matrix cracks, takes the non-dimensional form

$$\frac{\bar{E}\Delta\epsilon}{\beta\sigma_{mc}} = F_2\left(\frac{a}{t}, \frac{\sigma_0}{\beta\sigma_{mc}}, \frac{t}{L}\right). \tag{9}$$

Because of the nonlinearity of the fiber bridging law, the extra strain is no longer proportional to the applied stress σ. The total tensile strain ϵ at any time during the crack growth process is given by the sum

$$\epsilon = \frac{\sigma}{\bar{E}} + \Delta\epsilon. \tag{10}$$

If there exists residual stress in the composite, additional strain will be introduced due to release of such residual stress by the growth of matrix cracks, as will be included later.

For the convenience of presenting results it is useful to define the plane strain secant modulus $\bar{E}_{sec}$, which is also a function of a/t, $\sigma_0/(\beta\sigma_{mc})$ and t/L, as the ratio

$$\bar{E}_{sec} = \frac{\sigma}{\epsilon}. \tag{11}$$

Due to stress concentration arising from presence of the crack, the tensile stress in the bridging fibers is not simply σ/c_f, as it is well behind the crack tip in steady-state matrix cracking of unidirectional fiber-reinforced ceramics. In all cases studied, it is found that the maximum stress in the fibers always occurs in the bridging fibers located at the 90°/0° interfaces (the bridging/unbridging point). Denote this stress by σ_f; it is given by

$$\frac{c_f\sigma_f}{\beta\sigma_{mc}} = F_3\left(\frac{a}{t}, \frac{\sigma_0}{\beta\sigma_{mc}}, \frac{t}{L}\right). \tag{12}$$

Extensive results will be presented in next section for the non-dimensional functions defined in (8), (9), (11), and (12) for each of the two doubly periodic crack patterns. In addition, numerical examples will be presented to illustrate the influence of some of the parameters on the tensile behavior of laminated fibrous ceramic composites.

3. CRACK GROWTH PROCESS AND OVERALL TENSILE RESPONSE

A complete analysis of the crack growth problem with bridging fibers in the 0° plies is performed, as

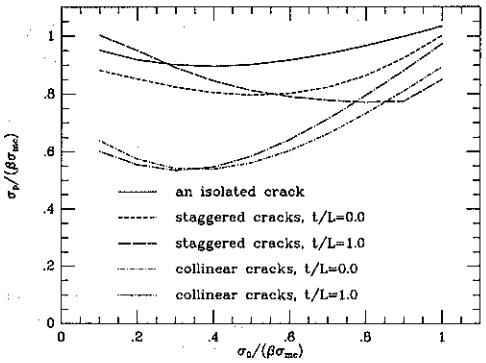

Fig. 4. Peak stress σ_p for several crack configurations.

described in the previous section. The crack growth process initiated from a single through-the-fibers crack in a uni-directional fiber-reinforced ceramic composite was discussed in [5], where emphasis was placed on the tensile strength of the composite. It was found in their analysis that a typical curve of applied stress σ vs matrix crack growth a/t always has following features, assuming no fibers break. Following initiation of the matrix crack growth at σ_0, the applied stress σ increases due to the constraining effects of crack-bridging fibers, until a peak value σ_p is reached. The applied stress σ then decreases as further growth continues with σ approaching the steady-state matrix cracking stress σ_{mc} asymptotically for $a \to \infty$. Thus σ_p is the largest stress the composite can sustain before the matrix crack is fully extended.

For the cross-ply laminate studied in the present work, matrix cracks in the 0° plies are bridged by intact fibers, but not those in the 90° plies. The largest stress a laminate can sustain before the matrix crack is fully extended, σ_p, is thus not necessarily same as that for a unidirectional fibrous composite. There are two possibilities. One is that the applied stress reaches the peak value before the matrix crack grows into the next 90° ply, and this peak value is the desired σ_p. Another possibility is that the applied stress σ is still increasing when the matrix crack reaches the next 90°/0° interface. Since no fiber-bridging constraint can occur in the 90° plies, the matrix crack will run dynamically across the next 90° under constant stress loading. Therefore in this situation the stress when crack reaches the 90°/0° interfaces is the peak stress, σ_p, the largest stress the laminate can sustain before the matrix is fully cracked. The peak value σ_p for one single crack in a 90° ply is plotted in Fig. 4 as solid line. It turns out that for most range of $\sigma_0/(\beta\sigma_{mc})$ studied, σ_p is associated with the second case mentioned above. Also plotted in Fig. 4 are peak values for other crack configurations. They will be explained later.

For the crack patterns shown in Fig. 2(a) and (b), a somewhat different crack growth process is found resulting from crack interaction. Results will be first presented for the collinear crack pattern [Fig. 2(a)], followed by those for the staggered crack pattern [Fig. 2(b)]. The influences of fiber bridging constraint and crack density on the tensile behavior of the laminates are also demonstrated. The last subsection will be devoted to the effect of the residual stress on the crack growth process and the overall tensile response.

3.1. Collinear crack pattern

The numerical results for the collinear crack arrays are given in Fig. 5, for the case that the crack density t/L is equal to 1. For other values of t/L, including the case of a single line of cracks with $t/L = 0$, the trends are similar. Figure 5(a) shows curves of the applied stress σ vs the matrix crack half length for a wide range of $\sigma_0/(\beta\sigma_{mc})$. These results are obtained by imposing the condition $K_I = K_{Ic}$ on the solution, as discussed. Crack growth into the adjacent 0° plies starts when the applied stress σ reaches a critical value which is somewhat below σ_0 due to crack interaction. This initiation stress is independent of $\sigma_0/(\beta\sigma_{mc})$. The actual initiation process of crack growth through an interface is very complicated. It depends on the elastic mismatches of the two materials as well as other features such as flaw size in a way which is not yet established. No attempt is made to address this issue since it is not critical in the present study. In this study, the interface is ignored as a potential barrier to the advancing matrix cracks.

As matrix cracks grow, the constraint of the crack-bridging fibers requires an increasing applied stress σ. However, interaction among cracks also becomes stronger, especially the stress intensity enhancement from the neighboring collinear cracks. The competition between fiber bridging constraint and crack interaction yields a peak value of σ occurring after an initial increase. This peak value, σ_p, is plotted in Fig. 4. Also plotted for comparison is the peak value for the case $t/L = 0$ (i.e. a simple array of collinear cracks). It is clear that the main effect of interaction arises from the collinear neighbors. After σ_p is reached, the matrix cracks grow under decreasing applied stress σ until the collinear cracks coalesce at middle of the 0° plies and the matrix becomes fully cracked.

The competition between fiber bridging constraint and crack interaction is evident in Fig. 5(a). The crack length at which σ_p is reached is longer for tougher bridging [smaller $\sigma_0/(\beta\sigma_{mc})$]. The corresponding extra tensile strains during the crack growth process are shown in Fig. 5(b). Unlike the applied stress σ, extra strains are monotonically increasing except near the coalescence of the cracks, where the applied stress σ drops sharply. To gain some feel of what a tensile stress–strain curve will look like during this crack growth process, we have also presented the results for the secant modulus $\bar{E}_{sec}$ as defined by (11), which is shown in Fig. 5(c). It is seen that the nonlinearity of tensile stress–strain behavior will be greater for softer bridging fibers [i.e. larger $\sigma_0/(\beta\sigma_{mc})$].

The tensile stresses σ_f in the fibers at the interface between the 0°/90° plies (where the fiber stress is maximum) is plotted in Fig. 5(d) as a function of a/t. for $\sigma_0/(\beta\sigma_{mc}) < 0.4$, the bridging stress $c_f\sigma_f$ is above matrix cracking stress σ_{mc}. Comparison of values in Fig. 5(d) with the fiber bundle strength will determine the likelihood of fiber fracture during the crack growth process for this type of crack pattern. Work currently in progress by the authors indicates that the stress concentration in the fibers at the 0°/90° interface is generally exaggerated by the line-spring model of bridging. Improved estimates of the stress concentration in the bridging fibers will be reported in a subsequent paper.

3.2. *Staggered crack pattern*

For the staggered crack pattern [shown in Fig. 2(b)], the collinear cracks are spaced every two plies as opposed to every other ply for the other doubly periodic cracks. Consequently matrix cracks will grow all the way through the adjacent 0° plies, and possibly extend into the next 90° plies. If they do extend into the next 90° plies, cracks will coalesce dynamically because of lack of fiber bridging constraint as well as stress intensity enhancement from neighboring collinear cracks. It is therefore only necessary to consider crack growth in the 0° plies.

For small crack density t/L, the crack growth behavior is determined by the competition between fiber bridging constraint and stress intensity enhancement from the neighboring collinear cracks. Figure 6 shows such a crack growth process for $t/L = 0.5$. The arrangement of the plots in Fig. 6 is the same as Fig. 5, except that the range of all the abscissae a/t are now from 1 to 3, reflecting crack extension through the entire 0° plies. This process is qualitatively similar to what was discussed in connection with

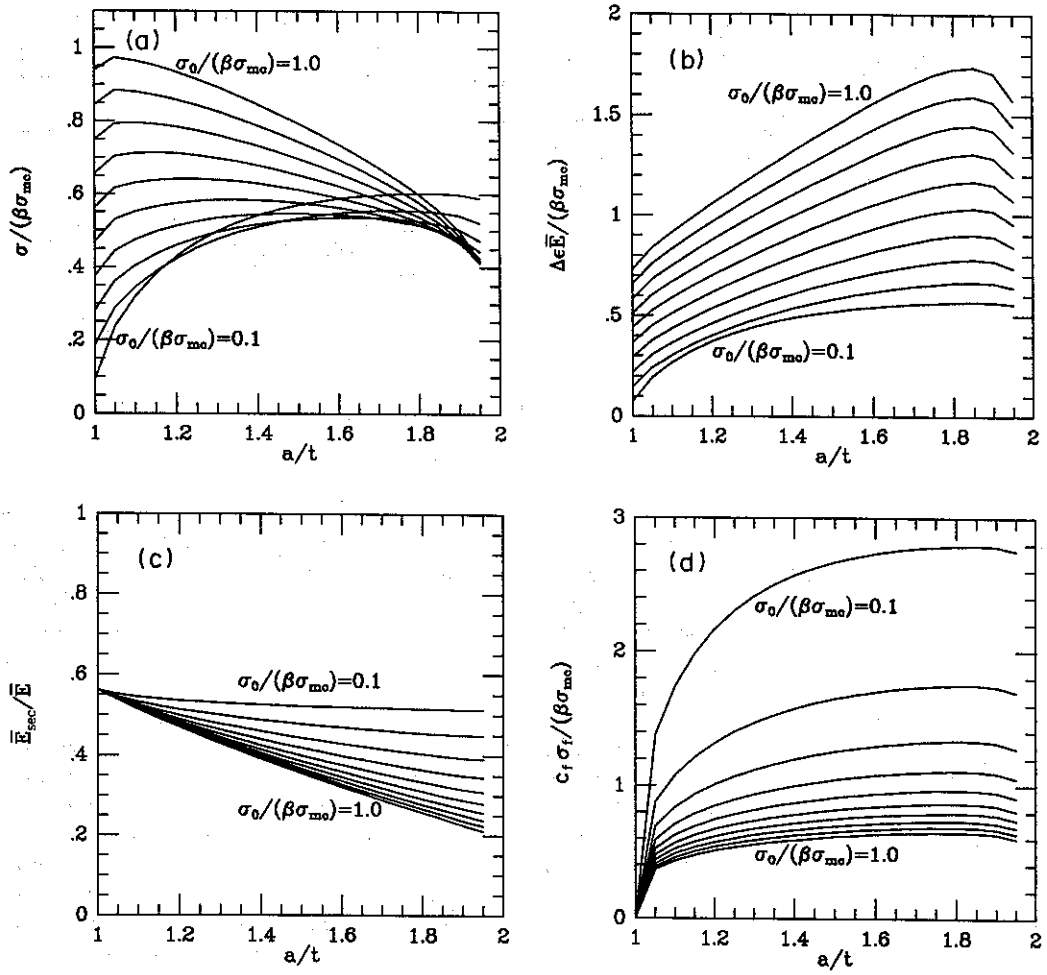

Fig. 5. Matrix crack process for collinear arrays, with crack density $t/L = 1.0$. (a) Applied stress vs matrix crack growth length. From bottom to top: $\sigma_0/(\beta\sigma_{mc}) = 0.1, 0.2, 0.3, 0.4, 0.5, 0.6, 0.7, 0.8, 0.9, 1.0$. (b) Inelastic strain vs matrix crack growth length. From bottom to top: $\sigma_0/(\beta\sigma_{mc}) = 0.1, 0.2, 0.3, 0.4, 0.5, 0.6, 0.7, 0.8, 0.9, 1.0$. (c) Secant modulus vs matrix crack growth length. From top to bottom: $\sigma_0/(\beta\sigma_{mc}) = 0.1, 0.2, 0.3, 0.4, 0.5, 0.6, 0.7, 0.8, 0.9, 1.0$. (d) Maximum fiber bridging stress vs matrix crack growth length. From top to bottom: $\sigma_0/(\beta\sigma_{mc}) = 0.1, 0.2, 0.3, 0.4, 0.5, 0.6, 0.7, 0.8, 0.9, 1.0$.

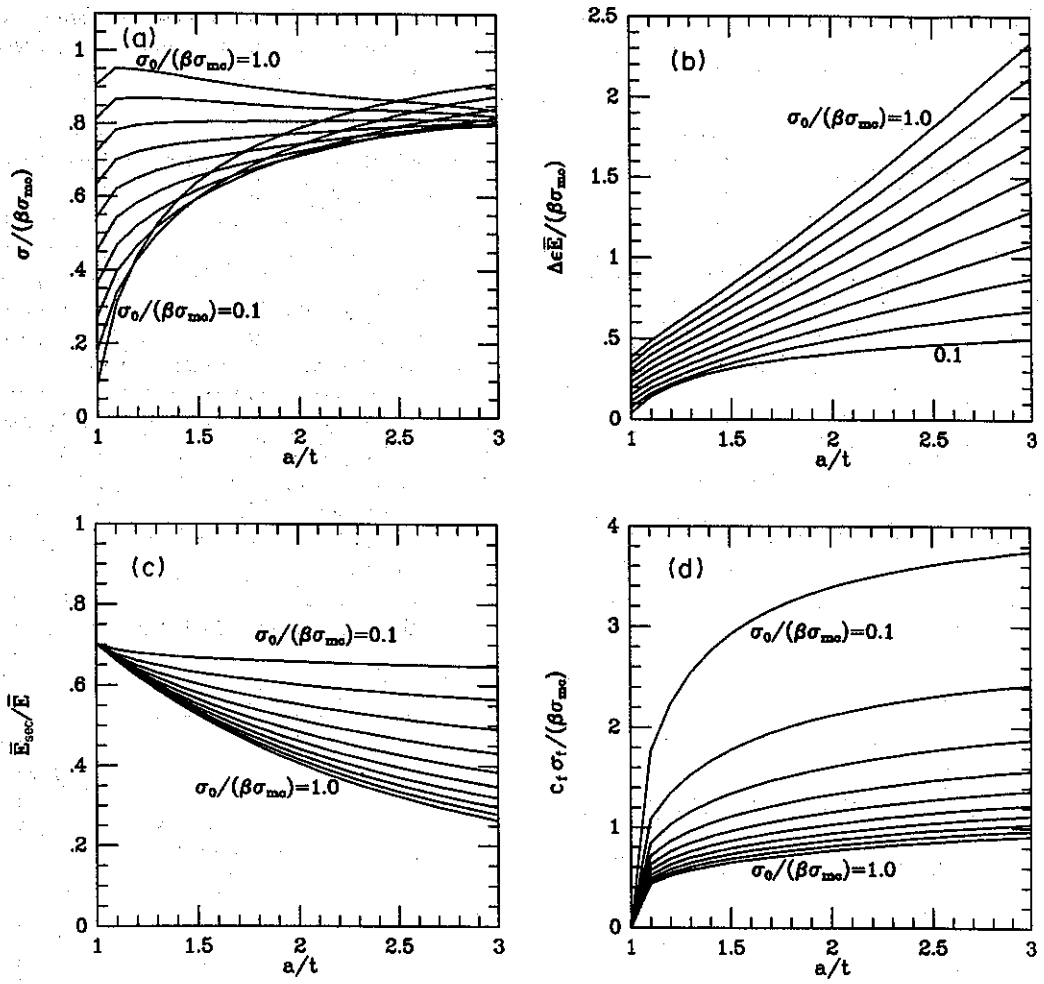

Fig. 6. Matrix crack process for staggered arrays, with crack density $t/L = 0.5$. (a)–(d): same arrangement as Fig. 5.

the collinear crack arrays, except that no crack coalescence occurs in this range.

A more interesting behavior is found if the crack density t/L becomes larger, as represented in Fig. 7 with $t/L = 1$. As matrix cracks pass the center of the 0° plies, the shielding effect from neighboring parallel cracks becomes strong, and the crack growth process is now governed by the competition among fiber bridging constraint, stress intensity enhancement from neighboring collinear cracks, *and* the shielding effect from parallel cracks. For a large crack density, the parallel cracks are sufficiently close that shielding becomes dominant. This is reflected in Fig. 7(a) by curves of applied stress σ vs crack length a. Beyerle *et al.* [1] reported from their experimental observations that some of the longer matrix cracks in the 0° plies seem to arrest under increasing load. The shielding effect on matrix crack growth displayed by the staggered crack pattern may explain this observation. The change of secant modulus $\bar{E}_{sec}$ for this crack pattern is much bigger than that for the regular crack pattern [compare Fig. 7(c) and Fig. 5(c), both for $t/L = 1$]. This is due to the fact that staggered cracks advanced all the way through the 0° plies, producing more inelastic strain.

The peak value stress σ_p for two typical staggered crack patterns are shown in Fig. 4, namely, the cases for $t/L = 0.0$ and $t/L = 1.0$. The difference between them is seen to be relatively small. It is clear from Fig. 4 that the most deleterious pattern is the collinear arrays. Even with $t/L = 0$, this pattern can result in a reduction of peak stress for matrix cracks to spread across the plies of almost 50% of σ_{mc}. This is not surprising since the collinear patterns shed all the load carried by the 90° plies into the 0° plies in the collinear plane, increasing the ligament loads by a factor of two. Collinear arrays are unlikely from a statistical point; and, as mentioned earlier, the staggered arrays are probably more realistic. The conclusion to be drawn from the peak stress plots in Fig. 4 is that the single layer, uni-directional matrix cracking stress σ_{mc} provides a reasonable estimate of the matrix cracking stress of the 0° plies in the

cross-ply composite, assuming the initiating cracks in the 90° plies do not line up in a collinear fashion. Considering the significantly lower peak stress associated with the collinear arrays, it may be worthwhile to investigate other related crack configurations which have a high likelihood of occurrence, e.g. two collinear cracks in the neighboring 90° plies.

This model has been used to generate overall tensile stress–strain behavior as dependent on several of the key parameters. In Fig. 8(a) plots are displayed of the normalized applied stress against the normalized strain for cases $t/L = 1$. The solid lines represent the behavior subsequent to initiation of crack growth into the 0° plies, which is the range considered in this paper. The initial elastic response, which is also shown as solid line, is terminated at the onset of tunnel cracks in the 90° plies. The transition response connecting the onset of tunnel cracking and the 0° ply cracking has not been computed here, but a typical response is shown as a dashed line curve. The effect of crack density on the overall stress–strain relation is illustrated in Fig. 8(b), where $\sigma_0/(\beta\sigma_{mc}) = 0.3$. The nonlinear behavior shown in these two figures is in general agreement with experimental data reported in the literature.

3.3. *Residual stress effect*

Residual stresses and strains are generally introduced during manufacturing process of a fiber-reinforced cross-ply laminate. As we discussed earlier, two types of residual stresses exist within different scales. When fibers and matrix are bonded together to form a uni-directional fibrous ply, residual stresses in axial and radial directions are introduced between fibers and matrix due to mismatch of their thermal properties. Another type of residual stresses exists at the ply level. When the plies are bonded together to form the cross-ply laninates, misfit strain results in residual stresses between plies. Both types of residual stresses can be rigorously modeled in the present analysis by a simple stress superposition and possible modification of fiber bridging law according to (4b), as discussed in Appendix A. For the sake of simplicity, only the results for residual stress between plies

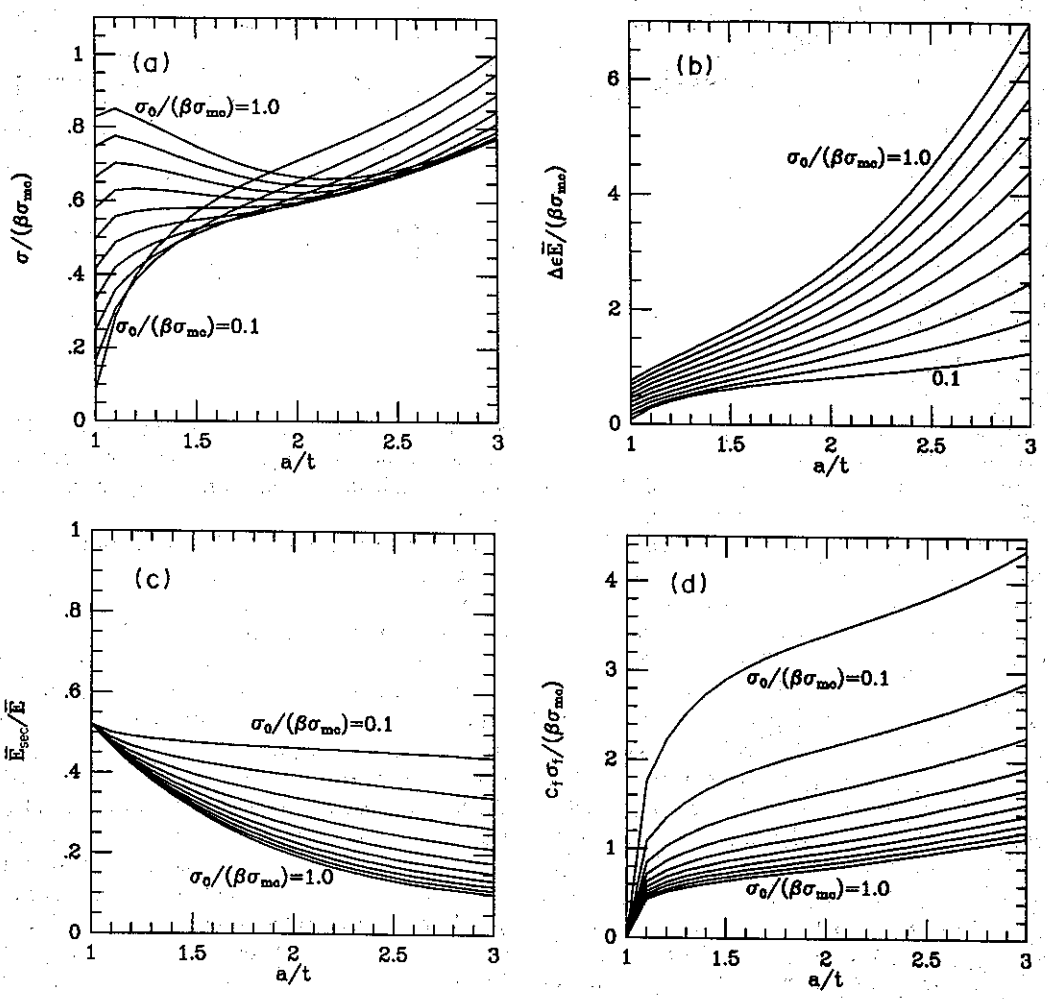

Fig. 7. Matrix crack process for staggered arrays, with crack density $t/L = 1.0$. (a)–(d): same arrangement as Fig. 5.

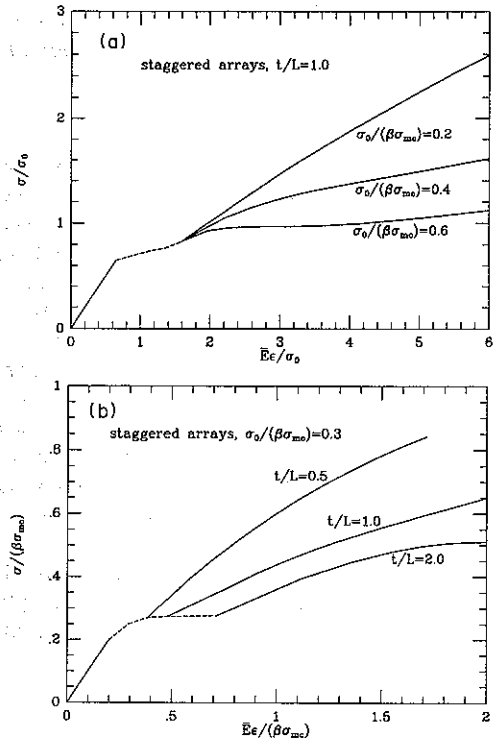

Fig. 8. (a) Stress–strain curves for different $\sigma_0/(\beta\sigma_{mc})$, staggered arrays, $t/L = 1.0$. (b) Stress–strain curves for different t/L, staggered arrays, $\sigma_0/(\beta\sigma_{mc}) = 0.3$.

will be presented in this paper. Consistent with our material approximation, we may assume that an initial, uniform residual tension σ_R exists in the 90° plies acting parallel to the applied stress, with same level of compression in the 0° plies.

Figure 9 shows the effect of a residual stress σ_R in the laminate, where σ_R is scaled with the reference stress σ_0. Since a residual tension is assumed in the 90° plies, the initiation value of σ is smaller than that if no residual stress were present. As matrix cracks grow, larger applied stress σ is required to overcome the residual compression in the 0° plies. The process is clearly indicated in Fig. 9(a). In any case, the secant modulus $\bar{E}_{sec}$ [shown in Fig. 9(b)] is smaller than that if no residual stresses are present. As matrix cracks become long, the differences in $\bar{E}_{sec}$ for various σ_R become small. The overall stress–strain response for different residual stresses are plotted in Fig. 9(c).

4. A NUMERICAL EXAMPLE

To obtain some real feel of our approach, a numerical calculation is performed for the CAS/SiC laminate discussed earlier. Based on its constituent properties, the values of relevant parameters are obtained to be

$$A = 0.97, \quad \bar{E} = 140\text{GPa}, \quad \sigma_0 = 88\text{ MPa},$$

$$\beta = 0.998, \quad \sigma_{mc} = 323\text{ MPa}.$$

The measured residual stress in the matrix σ_R^m is in the range 100–120 MPa. We shall use $\sigma_R^m = 110$ MPa in our calculation. The residual stress between plies $\sigma_R = 30$ MPa is also accounted for in the calculation.

Based on the above information, we are able to perform our calculation using the staggered crack pattern. The crack density is taken to be $t/L = 0.88$, which is the average saturation crack density measured in the experiment. The results for secant modulus $\bar{E}_{sec}$ vs applied stress σ are presented in Fig. 10 as solid lines. The experimental data from [1] are also plotted as solid dots. Also presented in Fig. 10 is the predicted secant modulus $\bar{E}_{sec}$ for crack density $t/L = 0.5$. The comparison with the experimental data suggests that in the stress range from 70 to 100 MPa the density of matrix cracks in the 90°

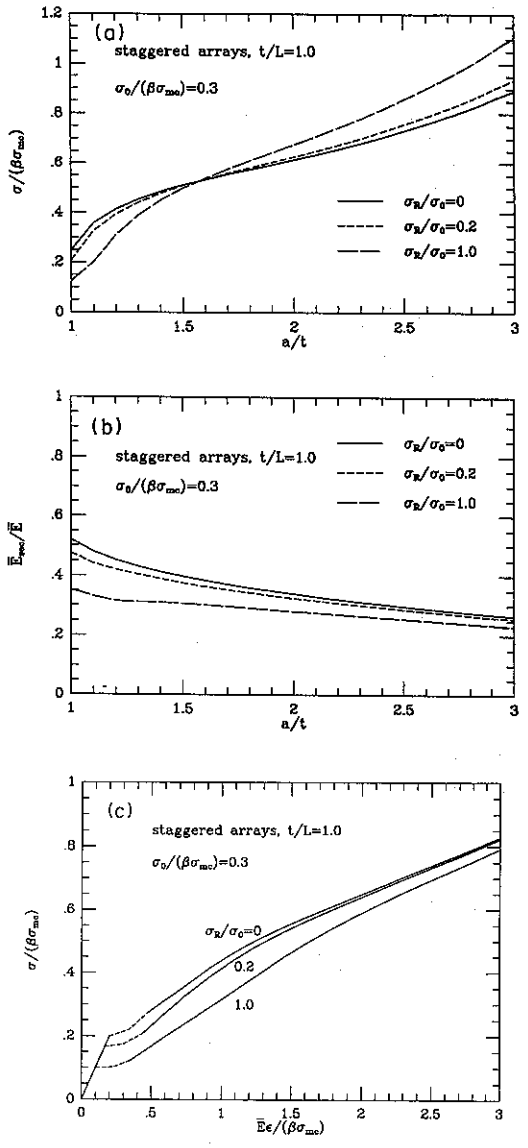

Fig. 9. Demonstration of effect of residual stress on matrix crack growth. (a) Applied stress vs matrix crack growth length. (b) Secant modulus vs matrix crack growth length. (c) Overall stress–strain response.

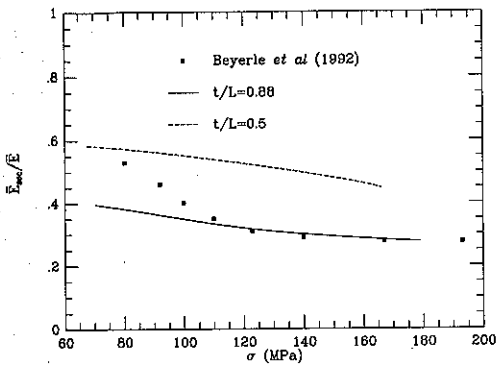

Fig. 10. Predicted secant modulus for a CAS/SiC laminate, compared with experimental data reported in Beyerle *et al.* (1992).

plies may be still increasing at the same time that matrix cracks are growing into the 0° plies.

Acknowledgements—This work was supported in part by the DARPA URI (Subagreement P.O. No. KK3007 with the University of California, Santa Barbara, ONR Prime Contract N00014-92-J-1808), by the Materials Research Lab. under Grant NSF-DMR-89-20490, and by the Division of Applied Sciences, Harvard University.

REFERENCES

1. D. S. Beyerle, S. M. Spearing and A. G. Evans, *J. Am. Ceram. Soc.* **75,** 3321 (1992).
2. N. Laws and G. J. Dvorak, *J. comp. Mater.* **22,** 900 (1988).
3. Z. C. Xia, R. R. Carr and J. W. Hutchinson, *Acta metall. mater.* **41,** 2365 (1993).
4. D. B. Marshall and B. N. Cox, *Acta metall.* **35,** 2607 (1987).
5. B. Budiansky and Y. L. Cui, *J. Mech. Phys. Solids* **42,** 1 (1994).
6. R. Hill, *Mech. Phys. Solids* **13,** 189 (1965).
7. J. Aveston, G. A. Cooper and A. Kelly, in *Conference Proceedings*, National Physical Laboratory, Guildford, p. 15. IPC Science & Technology Press (1971).
8. B. Budiansky, J. W. Hutchinson and A. G. Evans, *J. Mech. Phys. Solids* **34,** 167 (1986).
9. H. Tada, P. Paris and G. Irwin, *The Stress Analysis of Cracks Handbook*. Del Research, St Louis, Mo (1985).
10. D. B. Marshall, B. N. Cox and A. G. Evans, *Acta metall.* **33,** 2013 (1985).
11. D. B. Marshall and A. G. Evans, *Mater. Forum* **11,** 304 (1988).
12. J. R. Rice, in *Fracture* (edited by H. Liebowitz), Vol. II. Academic Press, New York (1968).
13. B. Budiansky and J. W. Hutchinson, *J. appl. Mech.* **45,** 267 (1978).
14. J. R. Rice, in *Fatigue Crack Propagation*. ASTM STP 415, p. 247 (1967).
15. Z. C. Xia and J. W. Hutchinson, *Int. J. Solids Struct.* In press.

APPENDIX A

Integral Equation Formulation for the Partially Bridged Matrix Cracking Problem

An integral equation for the partially bridged matrix cracking problem is formulated based on the dislocation distribution method (cf. [12]). In this method, cracks are represented as a superposition of continuously distributed dislocations. For the two doubly periodic crack patterns studied in this work, we only need to model half of a representative crack by distribution of edge dislocation $b(\eta) = b_y(\eta)$ (Fig. A1). The stress $\sigma_y(x)$ along crack face induced by edge dislocations $b(\eta)$ at $x = \eta$ and $-b(\eta)$ at $x = -\eta$ is given by

$$\sigma_y(x) = \frac{E}{4\pi}\left[\frac{1}{x-\eta} + A(x,\eta)\right]b(\eta). \tag{A1}$$

The kernel function $A(x, \eta)$ for the two crack patterns is given in Appendix B.

An integral equation is obtained by choosing the dislocation distribution to meet the traction conditions along the line of the crack and within crack bridging zone

$$\frac{E}{4\pi}\int_0^a \left\{\frac{1}{x-\eta} + A(x,\eta)\right\}b(\eta)\,d\eta = -\sigma^0(x) + p(x), \quad \text{for } 0 < x < a \tag{A2}$$

where $\sigma^0(x)$ is the stress normal to the crack surface prior to cracking, including remotely applied stress σ and the residual stress among plies, and $p(x)$ is the fiber bridging stress. Thus the right hand side of (A2) should be $-(\sigma + \sigma_R)$ for $0 < x < t$ (in the 90° plies), and $-(\sigma - \sigma_R) + p(x)$ for $t < x < a$ (in the 0° plies).

The crack opening displacement $\delta(x)$ is given by

$$\delta(x) = \int_x^a b(\eta)\,d\eta. \tag{A3}$$

Since only crack surfaces in the 0° plies (i.e. $t < x < a$, where t is half ply thickness) are bridged by fibers, the solution $b(\eta)$ to the integral equation exhibits a logarithm singularity at $\eta = t$ (cf [13, 14]; [9] for crack opening displacement solutions of Dugdale–Barenblatt model). Accordingly we can approximate $b(\eta)$ with the correct singularities built-in as

$$b(\eta) = \frac{4\pi\sigma_0}{E}\left\{c_0 \ln\frac{t-\eta}{t} + \sum_{j=1}^{N_1-1} c_j T_{j-1}\left(\frac{2\eta}{t} - 1\right)\right\} \quad \text{for } 0 \leqslant \eta < t$$

$$b(\eta) = \frac{4\pi\sigma_0}{E}\left\{d_0 \ln\frac{\eta-t}{a-t} + \sqrt{\frac{a-t}{2(a-\eta)}} \times \sum_{j=1}^{N_2-1} d_j T_{j-1}\left(\frac{2(\eta-t)}{a-t} - 1\right)\right\} \quad \text{for } t < \eta < a \tag{A4}$$

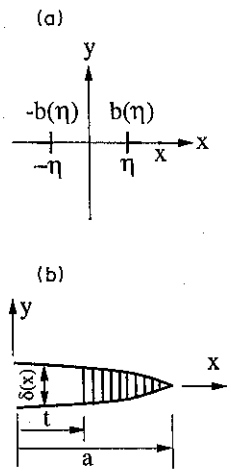

Fig. A1. (a) Dislocations used for each crack to obtain the kernel function in the integral equation. (b) A representative half crack modeled to formulate the integral equation.

where $T_j(\zeta)$ is the Chebyshev polynomial of first kind of degree j. c_j's and d_j's are (N_1+N_2) unknown coefficients which are to be determined.

The asymptotic behavior of $b(\eta)$ near crack tip $\eta=a$ gives the mode I stress intensity factor K_I in terms of the unknown coefficients as

$$K_I=\pi\sigma_0\sqrt{\pi(a-t)}\sum_{j=1}^{N_2-1}d_j. \tag{A5}$$

The crack opening displacement $\delta(x)$ for $t<x<a$ can be expressed as, by substituting (A4) into (A3)

$$\delta(x)=\frac{2\pi(a-t)\sigma_0}{E}\sum_{j=0}^{N_2-1}d_jf_j(x) \tag{A6}$$

where

$$f_0(x)=\int_s^1\ln\frac{1+\zeta}{2}\,d\zeta,\quad f_j(x)=\int_s^1\frac{T_{j-1}(\zeta)}{\sqrt{1-\zeta}}\,d\zeta,$$

and

$$s=\frac{2(x-t)}{a-t}-1. \tag{A7}$$

The fiber bridging stress $p(x)$ is given by, from (3) to (6) in the main text and (A6) above

$$\frac{p(x)}{\sigma_0}=\sqrt{\frac{2(a-t)}{3t}\left(\frac{\beta\sigma_{mc}}{\sigma_0}\right)^3\sum_{j=0}^{N_2-1}d_jf_j(x)}-\frac{\frac{E_L}{E_m}\sigma_R^m}{\sigma_0},$$

where

$$\beta=\left\{\frac{AE_L}{E(1-\nu_L^2)}\right\}^{1/3}. \tag{A8}$$

Substitution of (A4), (A8) into (A2) yields

$$\sum_{j=0}^{N_1-1}I_{1j}(x)c_j+\sum_{j=0}^{N_2-1}I_{2j}(x)d_j=-\frac{\sigma+\sigma_R}{\sigma_0},\quad \text{for } 0\leqslant x<t$$

$$\sum_{j=0}^{N_1-1}I_{3j}(x)c_j+\sum_{j=0}^{N_2-1}I_{4j}(x)d_j=-\frac{\sigma-\sigma_R}{\sigma_0}+\sqrt{\frac{2(a-t)}{3t}\left(\frac{\beta\sigma_{mc}}{\sigma_0}\right)^3\sum_{j=0}^{N_2-1}d_jf_j(x)}-\frac{\frac{E_L}{E_m}\sigma_R^m}{\sigma_0},\quad \text{for } t<x<a. \tag{A9}$$

The $I(x)$'s in the above equation are given by following integrals, after scaling the integration limits into $(-1, 1)$,

$$I_{10}(x),\ I_{30}(x)=\frac{t}{2}\int_{-1}^{1}\left[\frac{1}{x-\eta}+A(x,\eta)\right]\ln\frac{1-\zeta}{2}\,d\zeta$$

$$I_{1j}(x),\ I_{3j}(x)=\frac{t}{2}\int_{-1}^{1}\left[\frac{1}{x-\eta}+A(x,\eta)\right]T_{j-1}(\zeta)\,d\zeta \tag{A10}$$

where $\eta=t(1+\zeta)/2$, and

$$I_{20}(x),\ I_{40}(x)=\frac{a-t}{2}\int_{-1}^{1}\left[\frac{1}{x-\eta}+A(x,\eta)\right]\ln\frac{1+\zeta}{2}\,d\zeta$$

$$I_{2j}(x),\ I_{4j}(x)=\frac{a-t}{2}\int_{-1}^{1}\left[\frac{1}{x-\eta}+A(x,\eta)\right]\frac{T_{j-1}(\zeta)}{\sqrt{1-\zeta}}\,d\zeta \tag{A11}$$

where $\eta=t+(a-t)(1+\zeta)/2$. In the designated ranges of x, Cauchy Principle values are understood for $I_1(x)$'s and $I_4(x)$'s in (A10) and (A11).

The choice of allocation points for solving (A9) is somewhat arbitrary. Chebyshev points are used in our calculation

$$x_i=\frac{t}{2}\left\{1+\cos\left[\frac{(2i-1)\pi}{2N_1}\right]\right\},\quad i=1,2,\ldots,N_1\quad \text{for } 0\leqslant x<t$$

$$x_i=t+\frac{a-t}{2}\left\{1+\cos\left[\frac{(2i-1)\pi}{2N_2}\right]\right\},\quad i=1,2,\ldots,N_2\quad \text{for } t<x<a. \tag{A12}$$

An additional equation is obtained by imposing the crack growth condition $K_I=K_{Ic}$. The combination of (6) in the main text with (A5) gives

$$\sum_{j=1}^{N_2-1}d_j=\frac{1}{\pi}\sqrt{\frac{t}{a-t}}. \tag{A13}$$

Introduction of (N_1+N_2) allocation points in (A12) to (A9), together with (A13), provides (N_1+N_2+1) equations for solving (N_1+N_2+1) unknowns $c_0, c_1, \ldots, c_{N_1-1}$; $d_0, d_1, \ldots, d_{N_2-1}$, and remotely applies stress σ. This set of nonlinear equations are solved numerically by Newton's method.

It is not difficult to show that the inelastic strain $\Delta\epsilon$ introduced by matrix cracking can be obtained from

$$\Delta\epsilon=\frac{1}{4Lt}\int_0^a\delta(x)\,dx \tag{A14}$$

where $\delta(x)$ can be calculated from (A3).

APPENDIX B

Kernel Function $A(x,\eta)$

The kernel function $A(x,\eta)$ used in Appendix A to formulate the integral equation is obtained by superposition of the stress $\sigma_y(x)$ induced by arrays of periodic edge dislocations. The complete stress field for an array of periodic edge dislocations can be found in [15].

For collinear arrays

$$A(x,\eta)=\frac{\frac{\pi}{4t}}{\tan\frac{\pi}{4t}(x-\eta)}-\frac{1}{x-\eta}-\frac{\frac{\pi}{4t}}{\tan\frac{\pi}{4t}(x+\eta)}+\frac{\pi}{t}\sum_{y=2L,4L,\ldots}^{\infty}\left\{\frac{\sin\frac{\pi}{2t}(x-\eta)}{2\left[\cosh 2y-\cos\frac{\pi}{2t}(x-\eta)\right]}+\frac{y\sin\frac{\pi}{2t}(x-\eta)\sinh 2y}{\left[\cosh 2y-\cos\frac{\pi}{2t}(x-\eta)\right]^2}-\frac{\sin\frac{\pi}{2t}(x+\eta)}{2\left[\cosh 2y-\cos\frac{\pi}{2t}(x+\eta)\right]}-\frac{y\sin\frac{\pi}{2t}(x+\eta)\sinh 2y}{\left[\cosh 2y-\cos\frac{\pi}{2t}(x+\eta)\right]^2}\right\}. \tag{B1}$$

For staggered arrays

$$A(x,\eta)=\frac{\frac{\pi}{8t}}{\tan\frac{\pi}{8t}(x-\eta)}-\frac{1}{x-\eta}-\frac{\frac{\pi}{8t}}{\tan\frac{\pi}{8t}(x+\eta)}$$
$$+\frac{\pi}{2t}\sum_{y=2L,4L,\ldots}^{\infty}\left\{\frac{\sin\frac{\pi}{4t}(x-\eta)}{2\left[\cosh 2y-\cos\frac{\pi}{4t}(x-\eta)\right]}\right.$$
$$+\frac{y\sin\frac{\pi}{4t}(x-\eta)\sinh 2y}{\left[\cosh 2y-\cos\frac{\pi}{4t}(x-\eta)\right]^2}$$
$$-\frac{\sin\frac{\pi}{4t}(x+\eta)}{2\left[\cosh 2y-\cos\frac{\pi}{4t}(x+\eta)\right]}$$
$$\left.-\frac{y\sin\frac{\pi}{4t}(x+\eta)\sinh 2y}{\left[\cosh 2y-\cos\frac{\pi}{4t}(x+\eta)\right]^2}\right\}$$
$$-\frac{\pi}{2t}\sum_{y=L,3L,\ldots}^{\infty}\left\{\frac{\sin\frac{\pi}{4t}(x-\eta)}{2\left[\cosh 2y+\cos\frac{\pi}{4t}(x-\eta)\right]}\right.$$
$$+\frac{y\sin\frac{\pi}{4t}(x-\eta)\sinh 2y}{\left[\cosh 2y+\cos\frac{\pi}{4t}(x-\eta)\right]^2}$$
$$-\frac{\sin\frac{\pi}{4t}(x+\eta)}{2\left[\cosh 2y+\cos\frac{\pi}{4t}(x+\eta)\right]}$$
$$\left.-\frac{y\sin\frac{\pi}{4t}(x+\eta)\sinh 2y}{\left[\cosh 2y+\cos\frac{\pi}{4t}(x+\eta)\right]^2}\right\}. \quad \text{(B2)}$$

APPENDIX C

Nomenclature (Partial Listing)

a = half crack length
c_f, c_m = fiber and matrix volume concentration ($c_f + c_m = 1$)
t = half ply thickness
A = orthotropy factor
E_f, E_m = Young's moduli of fibers and matrix
$\bar{E}, E_{sec}$ = average Young's modulus of plane strain, secant modulus of the cracked composite
L = half crack spacing
R = fiber radius
β = a material parameter [defined in equation (7)]
ϵ = total tensile strain
$\Delta\epsilon$ = extra tensile strain (inelastic strain due to cracking)
σ_f = tensile stress in bridging fibers
σ_p = largest stress a composite can sustain before the matrix crack is fully extended
σ_R = residual stress
τ = fiber/matrix sliding shear resistance
Γ_m = critical energy release rate of the matrix
E_L, ν_L, μ_L = longitudinal Young's modulus, Poisson's ratio and shear modulus of a single ply
E_T, ν_T, μ_T = transverse Young's modulus, Poisson's ratio and shear modulus of a single ply